

Interaction of supersonic molecular beam with low-temperature plasma

Dong Liu(刘东), Guo-Feng Qu(曲国峰), Zhan-Hui Wang(王占辉), Hua-Jie Wang(王华杰), Hao Liu(刘灏), Yi-Zhou Wang(王艺舟), Zi-Xu Xu(徐子虚), Min Li(李敏), Chao-Wen Yang(杨朝文), Xing-Quan Liu(刘星泉), Wei-Ping Lin(林炜平), Min Yan(颜敏), Yu Huang(黄宇), Yu-Xuan Zhu(朱宇轩), Min Xu(许敏), Ji-Feng Han(韩纪锋)

Citation: Chin. Phys. B . 2020, 29(6): 065208 . **doi:** 10.1088/1674-1056/ab8457
Journal homepage: http://cpb.iphy.ac.cn; http://iopscience.iop.org/cpb

What follows is a list of articles you may be interested in

Effects of secondary electron emission on plasma characteristics in dual-frequency atmospheric pressure helium discharge by fluid modeling

Yi-Nan Wang(王一男), Shuai-Xing Li(李帅星), Yue Liu(刘悦), Li Wang(王莉)

Chin. Phys. B . 2019, 28(2): 025202 . **doi:** 10.1088/1674-1056/28/2/025202

Factors affecting improvement of fluorescence intensity of quartet and doublet state of NO diatomic molecule excited by glow discharge

Ahmed Asaad I Khalil, Reem Al-Tuwirqi, Mohammed A Gondal, Noura Al-Suliman

Chin. Phys. B . 2018, 27(8): 085202 . **doi:** 10.1088/1674-1056/27/8/085202

Numerical study on discharge characteristics influenced by secondary electron emission in capacitive RF argon glow discharges by fluid modeling

Lu-Lu Zhao(赵璐璐), Yue Liu(刘悦), Tagra Samir

Chin. Phys. B . 2018, 27(2): 025201 . **doi:** 10.1088/1674-1056/27/2/025201

Understanding hydrogen plasma processes based on the diagnostic results of 2.45 GHz ECRIS at Peking University

Wen-Bin Wu(武文斌), Hai-Tao Ren(任海涛), Shi-Xiang Peng(彭士香), Yuan Xu(徐源), Jia-Mei Wen(温佳美), Jiang Sun(孙江), Ai-Lin Zhang(张艾霖), Tao Zhang(张滔), Jing-Feng Zhang(张景丰), Jia-Er Chen(陈佳洱)

Chin. Phys. B . 2017, 26(9): 095204 . **doi:** 10.1088/1674-1056/26/9/095204

Simulations of fast component and slow component of SMBI on HL-2A tokamak

Yong-Fu Shi(史永福), Zhan-Hui Wang(王占辉), Qi-Long Ren(任启龙), Ai-Ping Sun(孙爱萍), De-Liang Yu(余德良), Wen-Feng Guo(郭文峰), Min Xu(许敏)

Chin. Phys. B . 2017, 26(5): 055201 . **doi:** 10.1088/1674-1056/26/5/055201

Interaction of supersonic molecular beam with low-temperature plasma*

Dong Liu(刘东)[1], Guo-Feng Qu(曲国峰)[1,†], Zhan-Hui Wang(王占辉)[2], Hua-Jie Wang(王华杰)[2], Hao Liu(刘灏)[2], Yi-Zhou Wang(王艺舟)[1], Zi-Xu Xu(徐子虚)[1], Min Li(李敏)[1], Chao-Wen Yang(杨朝文)[1], Xing-Quan Liu(刘星泉)[1], Wei-Ping Lin(林炜平)[1], Min Yan(颜敏)[1], Yu Huang(黄宇)[1], Yu-Xuan Zhu(朱宇轩)[2], Min Xu(许敏)[2], and Ji-Feng Han(韩纪锋)[1,‡]

[1] *Key Laboratory of Radiation Physics and Technology of the Ministry of Education, Institute of Nuclear Science and Technology, College of Physics, Sichuan University, Chengdu* 610064, *China*
[2] *Southwestern Institute of Physics, Chengdu* 610041, *China*

(Received 24 January 2020; revised manuscript received 5 March 2020; accepted manuscript online 30 March 2020)

The interaction between the supersonic molecular beam (SMB) and the low-temperature plasma is a critical issue for the diagnosis and fueling in the Tokamak device. In this work, the interaction process between the argon SMB and the argon plasma is studied by a high-speed camera based on the Linear Experimental Advanced Device (LEAD) in Southwestern Institute of Physics, China. It is found that the high-density SMB can extinct the plasma temporarily and change the distribution of the plasma density significantly, while the low-density SMB can hardly affect the distribution of plasma density. This can be used as an effective diagnostic technique to study the evolution of plasma density in the interaction between the SMB and plasma. Moreover, the related simulation based on this experiment is carried out to better understand the evolution of electron density and ion density in the interaction. The simulation results can be used to analyze and explain the experimental results well.

Keywords: supersonic molecular beam, low-temperature plasma, emission, electron density diagnosis, high-speed camera

PACS: 52.40.Mj, 37.20.+j, 52.25.–b, 07.05.–t **DOI:** 10.1088/1674-1056/ab8457

1. Introduction

In the field of controlled nuclear fusion, supersonic molecular beam injection (SMBI)[1] is an effective fueling method in Tokamak due to its high fueling efficiency compared with gas puffing (GP)[2,3] and low cost compared with pellet injection (PI).[4] Therefore, the interaction between the supersonic molecular beam (SMB) and plasma is an important issue in both fueling and diagnosis for Tokamak. And in the interaction, the SMBI is a diagnosis technology[5,6] for the interaction process between the SMB and the edge plasma in the Tokamak. The density[7,8] and velocity[9] of SMB as well as the plasma temperature and density are key parameters in the interaction. In traditional experiments, the SMB is directly injected into the Tokamak and interacted with plasma in order to study the interaction process.

There are many experiments on the interaction between the SMB and plasma in the Tokamak such as HL-1M,[5,10] HL-2A,[11–13] EAST,[14] and JT-60U.[15] These experiments focused on a global effect of the interaction between the SMB and plasma in the Tokamak. For example, in the HL-2A, the injection depth was found to be consistent with the fueling efficiency of SMBI in Tokamak. The injection depth and fueling efficiency were determined by the density and temperature of the plasma as well as the density and velocity of SMB.[16] And the H_α emission image was used to measure the injection depth. According to the result of Ref. [16], in HL-2A, the injection depth was deeper when the electron density or temperature was lower. If the clusters were available in the SMB, the injection depth could be further enhanced. In addition, there were some relative simulations[6,17–20] about the injection process of SMB based on the parameters of HL-2A. The results of simulation proved the above conclusions about injection depth of SMB.

However, the physical properties of plasma such as temperature and density are complicated and varied in the traditional Tokamaks. For example, in the HL-2A, the temperature of edge plasma is about 10 eV but it could reach to 725 eV or even higher in the core plasma,[18] indicating that there is a large gradient of plasma temperature in the Tokamak. Thus, in the process of SMBI, the detailed mechanism and process of the interaction between the SMB and the edge plasma is difficult to study in depth in Tokamak. In the present experiment, a low-temperature plasma column (about 5 eV) is generated in the Linear Experimental Advanced Device (LEAD), which

*Project supported by the National Natural Science Foundation of China (Grant Nos. 11575121, 11275133, and 11575055) and the National Magnetic Confinement Fusion Program of China (Grant No. 2014GB125004).

†Corresponding author. E-mail: quguofeng@scu.edu.cn
‡Corresponding author. E-mail: hanjf@scu.edu.cn

© 2020 Chinese Physical Society and IOP Publishing Ltd

was established in 2018.[21] In this device, a magnetic field (about 0.04 Tesla) with linear configuration is much weaker than that in the traditional Tokamak (several Tesla). In this work, the experiment based on the low-temperature plasma and lower magnetic field is carried out to study the process of interaction between SMB and edge plasma, and explain the relative physical mechanism. The physical parameters such as density and temperature of plasma in the LEAD are close to those of the normal edge plasma in the real Tokamak. Therefore, this experiment could be used to simulate the interaction between the SMB and edge plasma in the Tokamak, and the results are valuable supplements for the research of the interaction between the atom/molecule and plasma. And this study of interaction process can conduce to better understanding of the process of SMBI in the Tokamak.

2. Experimental setups

A schematic diagram of this experiment is shown in Fig. 1. The whole experimental setup could be divided into two parts: the SMB and the plasma. And they were connected by a flight tube (with an inner diameter of 80 mm). In this experiment, argon was used as the experimental gas for both SMB and plasma. The SMB was produced by opening a cylindrical nozzle (type: Series 9, Park Hannifn Corporation) in vacuum. Then the central part of SMB was injected into the plasma through a skimmer with the throat diameter of 3 mm. The open time of the nozzle was fixed at 3 ms. In the diagram, the horizontal Y direction is the flight direction of SMB, the horizontal Z direction ("⊗" in Fig. 1) is the flow direction of the plasma, and the X direction is the vertical direction.

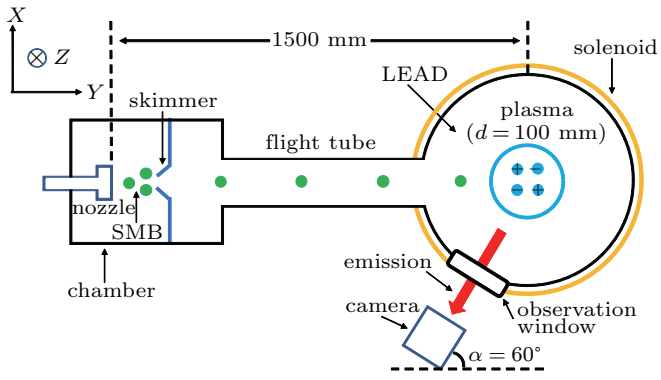


Fig. 1. Schematic diagram of the experimental setup.

For the LEAD, the vacuum chamber was divided into two parts, a small cylinder with a diameter of 400 mm and a large cylinder with a diameter of 900 mm.[21] And the total length of vacuum chamber was 3.5 m. In this experiment, the SMB was injected into the small cylinder part of the LEAD. The interaction position was about 1500-mm downstream from the radio frequency power source of the plasma, and about 1500-mm downstream from the nozzle of the SMB. The cross section of the small cylinder is shown in the right part of Fig. 1, denoted as one black circle. The interaction images were taken by a high-speed camera through a circular observation window with a diameter of 100 mm. The observation angle (α in Fig. 1), which was defined as the angle between the observation direction and the Y axis, was 60°.

In the interaction between the SMB and plasma, the argon atoms in the SMB can be excited to a high energy level by the electrons, and emission was generated in the deexcitation process. And the emitted photons were collected by the camera. The shooting speed of 3200 fps (frame per second) was used to take the interaction image with a resolution of 1280×720.

2.1. Parameters of argon SMB

In the experiment, the SMB density could be adjusted by changing the stagnation pressure of the gas jet or the distance between the nozzle and skimmer. The stagnation pressure (P) could be adjusted from 10 bar (1 bar = 10^5 Pa) to 50 bar, while the distance between the nozzle and skimmer (abbreviated as D in this work) was fixed at three values, which were 5 mm, 10 mm, and 15 mm. The SMB density in the region of interaction was measured by a microphone according to Refs. [7–9]. The SMB density followed a Gaussian distribution. The central density of the SMB *versus* stagnation pressure for three skimmer setups is shown in Fig. 2.

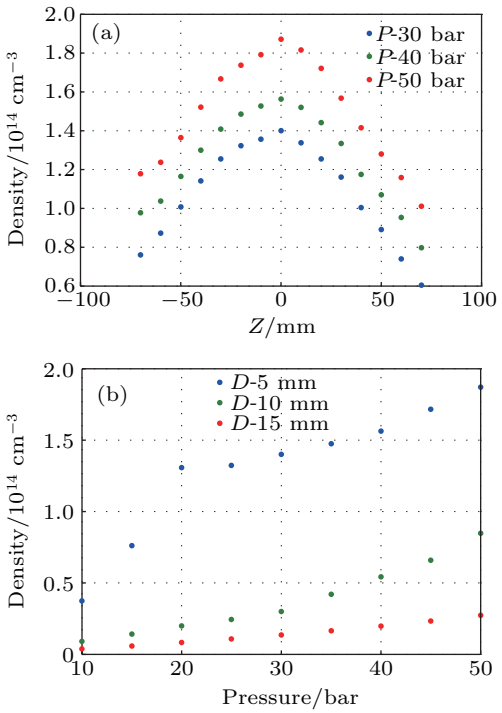


Fig. 2. Radial (along X or Z axis) distribution of (a) SMB density at 1500-mm downstream from nozzle under three different stagnation pressures and (b) central SMB density at different stagnation pressures for three skimmer setups with distance between nozzle and skimmer (D) being 5 mm, 10 mm, and 15 mm, respectively.

It is obvious that the density is in a range of 10^{12} cm^{-3}–10^{14} cm^{-3}, which increases with the stagnation pressure. And

the density is much lower when the distance between the nozzle and skimmer becomes longer. It is found that the SMB density in the radial direction (Z axis) conforms to the Gaussian distribution and the full width at half maximum (FWHM) is in a range from about 110 mm to 160 mm.

2.2. Parameters of argon plasma

A radio frequency (RF) power source was adopted in the LEAD to generate the argon plasma by discharging the argon gas.[22] The plasma density could be adjusted by changing the RF power of the plasma source, which could be adjusted from 1000 W to 3000 W[23–25] in this experiment. The argon gas pressure in the LEAD was kept at about 0.5 Pa. The average electron temperature in the plasma was about 5 eV, while the ion temperature could be neglected. The diameter of plasma column was about 100 mm.

An image without gas jet was shown in Fig. 3(a). The outer circle in the image is the boundary of the observation window. The emission was generated by the deexcitation of argon atoms/ions in plasma column. The butterfly shaped emission image might be caused by the reflection from the flange which was opposite to the observation window. Since the middle area was less affected by the reflection, the emission profile in this area (the area within the two black lines in Fig. 3(a)) is calculated in detail. The distribution of emission can represent the radial distribution of electron density in the plasma column. The FWHM of emission distribution is in a range from about 30 mm to 40 mm, which should be equal to the FWHM of the electron density distribution.

The electron density could be calculated by several parameters of experiment. In Ref [24], an equation to calculate the total number of electrons (N_e) in the entire plasma region was proposed and shown in Eq. (1), where the number of electrons is determined by the RF power (P_{inp}), the radius of plasma column (a), and the total length of plasma column (L) below

$$\frac{N_e}{P_{inp}} = ka^2L, \tag{1}$$

where k is an empirical parameter which is about 1.65×10^{15} $W^{-1}\cdot m^{-3}$. Thus, the electron density can be calculated by N_e and the spatial density distribution in Fig. 3(b). The calculated central electron density is about 1.97×10^{12} cm^{-3} for an RF power of 1000 W. The radial distribution (Y axis) of electron density is shown in Fig. 3(b). The electron density at each radial position can be calculated based on the radial distribution of electron density. In addition, the electron density is proportional to RF power as shown in Eq. (1) and the electron density values for other RF power are calculated accordingly.

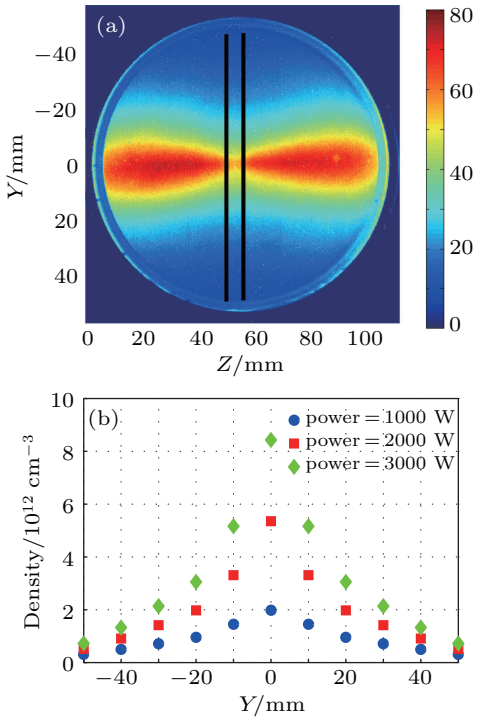


Fig. 3. (a) Emission image without gas jet with RF power being 1000 W and RF source being about 1500 mm upstream from left side of image, and (b) corresponding distribution of electron density in plasma column for three different power values.

3. Experimental and simulation results

3.1. Physical model and simulation

The experiment and analysis are mainly based on the emission images obtained from the camera. When the argon atom in the SMB is excited to higher excitation state by the electron in the plasma, a photon might be generated during the deexcitation. For the electron with 5 eV, the common emission is the well-known argon "red" lines, which are generated in the transition between the 4s and 4p configurations of argon atom.[26] The corresponding wavelengths of this emission are likely to be in a range of 760 nm–780 nm.[27] And relative electron excitation cross section is on the order of 10^{-15} cm^2 for the 5-eV electrons. The emission intensity is proportional to the density of SMB, the density of electron and the emission cross section.

For the interaction between the argon atom and argon ion, the elastic scattering, momentum transfer, and charge transfer are the three main interaction modes.[28] The elastic scattering is the dominant interaction mode for energy lower than 0.1 eV whose cross section is on the order of 10^{-13} cm^2. While the cross section of momentum transfer and charge transfer are about 10^{-14} cm^2 and 10^{-15} cm^2 in this energy range, respectively. In this experiment, the temperature of argon ions and atoms are both lower than 0.1 eV. Therefore, the elastic scattering is the main mode, and the injection flux of SMB might decrease during its interacting with ions in the plasma.

A relative simulation in three-dimensional space is conducted to better understand the experimental results and study the variation of density of electron and ion in the plasma during the whole interaction. In the simulation, the minimum length step is fixed at 0.4 mm and the simulated space is a cube of 100 mm^3. The density of electron and ion in the plasma are the same before the injection flux interacting with the plasma. In the interaction, the SMB flies along Y axis from the top to the bottom in minimum length steps. And the SMB collides with ions along the path, leading the ion density and SMB flux to change. The electron density may decrease due to the emission, and the electrons from the plasma source are able to diffuse along the Z axis slowly due to the variation of electron density. The ion can be considered to be static and its diffusion is neglected in simulation because of its much lower velocity. The SMB is injected into the plasma in the Y direction and argon atoms interact with electrons and ions in the plasma.

In the simulated interaction, for a fixed moment (T) and a fixed position (L), the emission and collision are given below:

$$I_{\rm emi}^{L,T} = \sigma_{\rm emi}\rho_{\rm e}^{L,T}F_{\rm SMB}^{L,T}T_{\rm unit}L_{\rm unit}^3, \tag{2}$$

$$I_{\rm col}^{L,T} = \sigma_{\rm col}\rho_{\rm ion}^{L,T}F_{\rm SMB}^{L,T}T_{\rm unit}, \tag{3}$$

where $I_{\rm emi}^{L,T}$ is the emission intensity which is defined as the number of photons at moment T and position L; $\sigma_{\rm emi}$ and $\sigma_{\rm col}$ are corresponding to the emission cross section and elastic collision cross section, respectively; $\rho_{\rm e}^{L,T}$ and $\rho_{\rm ion}^{L,T}$ are the electron density and ion density, respectively; $F_{\rm SMB}^{L,T}$ is the SMB flux which is defined as the product of the density and velocity in the interaction; $L_{\rm unit}$ and $T_{\rm unit}$ are the unit length and unit time, respectively; $I_{\rm col}^{L,T}$ is defined as the density of collision pairs between the atom and ion. In order to compare with the image of emission in the experiment, the number of photons, density of electrons and ions in the simulation are averaged in the X axis separately. Thus, the two-dimensional simulated images about the plasma density can be acquired.

The electron density and ion density are changed continuously in the whole interaction process. The relevant equations are shown as follows:.

$$\rho_{\rm e}^{L,T} = \rho_{\rm e}^{T-1} - I_{\rm emi}^{L,T}/L_{\rm unit}^3 + \rho_{\rm dif}^{L}, \tag{4}$$

$$\rho_{\rm ion}^{L,T} = \rho_{\rm ion}^{L,T-1} + I_{\rm col}^{L-1,T-1} - I_{\rm col}^{L,T}, \tag{5}$$

$$F_{\rm SMB}^{L,T} = F_{\rm SMB}^{L,T-1} - I_{\rm col}^{L,T}. \tag{6}$$

In Eq. (4), the variation of electron density is determined by the loss of emission and the diffusion from plasma source. The $\rho_{\rm dif}^{L}$ is the diffused electron density, which is viewed as constant at a fixed moment, and $\rho_{\rm dif}^{L}$ conforms to the Gaussian distribution in the radial direction of plasma (Y axis) and decreases along the direction of electron diffusion (Z axis). In Eq. (5), the variation of ion density is determined by the collision and the addition from the former step ($I_{\rm col}^{L-1,T-1}$). Because the ions in the former step will fly into this position due to collision. In Eq. (6), the variation of SMB flux is determined by the collision with ion ($I_{\rm col}^{L,T}$). The five relevant equations (Eqs. (2)–(6)) are used to calculate the plasma density in the simulation.

3.2. Plasma extinction by high-density SMB

When high-density SMB interacts with plasma column, the electrons in the plasma can be depleted fast and generate a number of photons. The plasma is extincted temperately during the gas jet. A series of images is shown in Fig. 4, which can represent the interaction between the SMB and plasma. The pixel values of image represent the number of photons which is recorded by the camera. The SMB flies along the Y axis from the top to the bottom while the plasma flows along the Z axis from the left to the right. It is obvious that the emission intensity in the center area continues decreasing in Fig. 4 and shifting to the left side gradually, which is corresponding to the scenario of the plasma source.

When the SMB is just injected into the plasma (T_0 is the start time (0 ms) in this work), the emission intensity increases quickly, and the emission intensity reaches a strongest value after 0.3215 ms, which is shown in Fig. 4(a). It is found that the emission intensity has a symmetrical distribution in both Z-axis and Y-axis directions. This symmetrical distribution is generated based on the symmetrical distribution of SMB density and electron density. The FWHM of emission area in the Y-axis direction is about 30 mm, which is almost equal to the distribution size of electron density. And the FWHM of emission area in the Z-axis direction is about 80 mm, which is smaller than that of SMB. This means that the spatial distribution of SMB inside the plasma becomes narrow.

In Fig. 4(b) which is about 1.25 ms after T_0, it is found that the emission intensity decreases slightly and emission center shifts from the center to the left side. In addition, the size of emission area becomes smaller than what is shown in Fig. 4(a). The reason is that the density of electrons which can lead the emission to continue decreasing in the process of interaction. Since more electrons can be supplemented into the left area from the plasma source, which would render the emission much stronger on the left side. In Fig. 4(c) which is about 2.1875 ms after T_0, the emission intensity is much weaker than that in Fig. 4(a) and the emission center continues shifting to the left side. Much more electrons are depleted by the SMB and less electrons could be supplemented by the source. And only a few electrons exist on the right side because the supplement of electron is lower than on the left side. Thus, low-

density electrons make the emission intensity much weaker. In Fig. 4(d) which is about 3.125 ms after T_0, both the emission area and the maximum emission intensity are only half that in Fig. 4(a). There is almost no emission on the right side, which means that all the electrons are depleted by the SMB and the plasma is extinct temporarily.

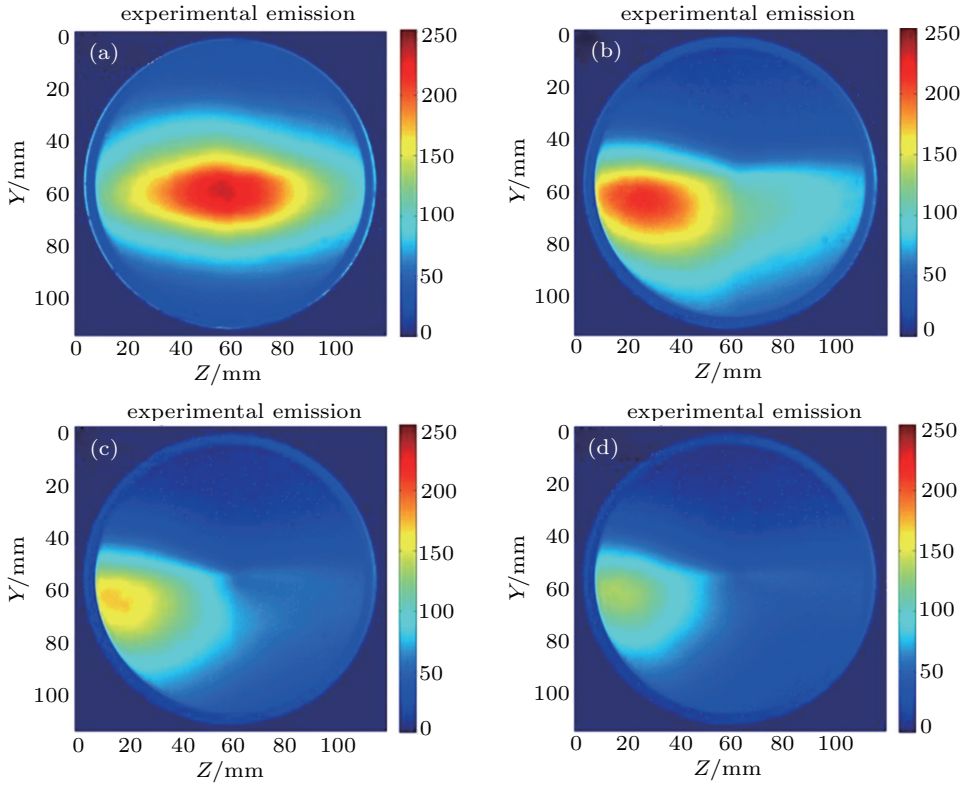


Fig. 4. A series of experimental emission images for high-density SMB, plasma extinct temporarily. Distance between nozzle and skimmer is 5 mm, stagnation pressure 30 bar, and central density of SMB about 1.40×10^{14} cm^{-3}, RF power 1000 W and initial central plasma density about 1.97×10^{12} cm^{-3}, at time (a) 0.3125 ms, (b) 1.2500 ms, (c) 2.1875 ms, and (d) 3.1250 ms after SMB has hit plasma column. Exposure time of each image is 0.2 ms.

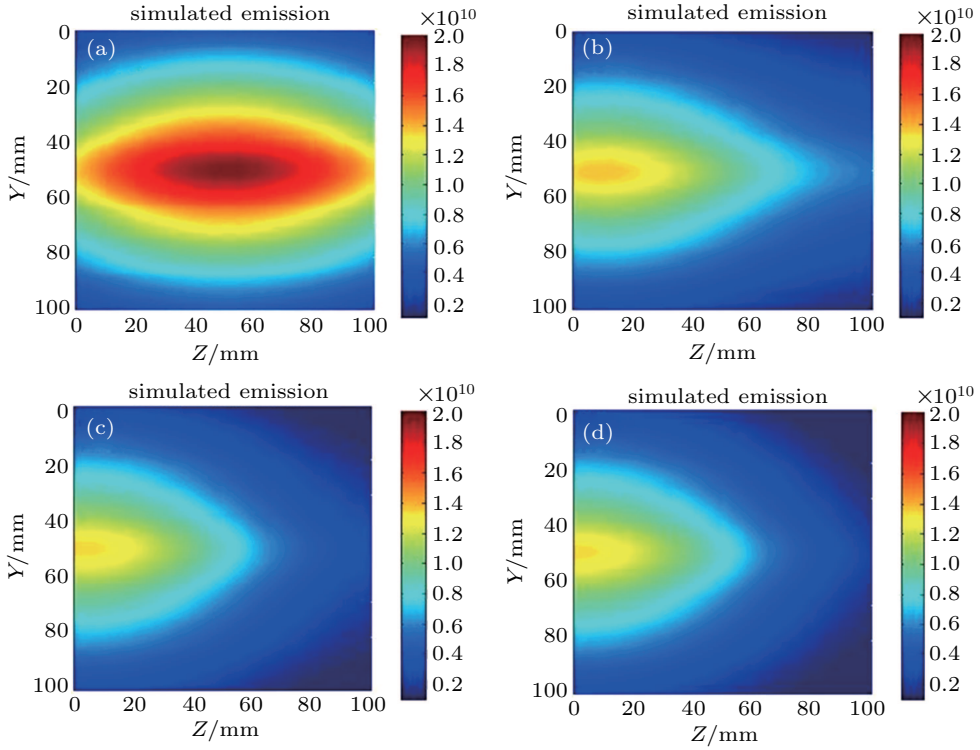


Fig. 5. A series of emission images by simulation for high-density SMB. Distance between nozzle and skimmer is 5 mm, the stagnation pressure 30 bar, RF power 1000 W. at time (a) 0.2 ms, (b) 1.2 ms, (c) 2.2 ms, and (d) 3.2 ms after SMB has hit plasma column.

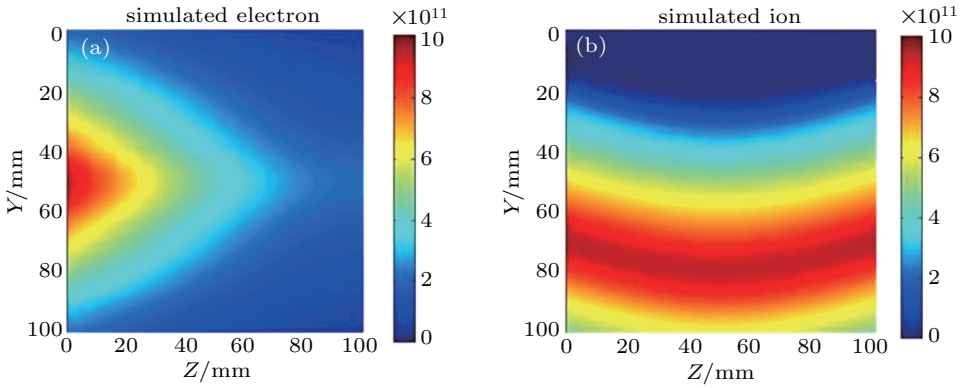


Fig. 6. Simulated (a) electron density and (b) ion density at 2.2 ms for high-density SMB (Distance between nozzle and skimmer is 5 mm, the stagnation pressure 30 bar, and RF power 1000 W).

The interaction process under the condition of Fig. 4 is simulated in detail. And the simulated a series of emission images is shown in Fig. 5. A phenomenon in Fig. 4 is found to be similar to that in Fig. 5, where the maximum emission intensity decreases and the center of emission shifts to the left side gradually. Therefore, this simple simulation is able to explain the experimental results. It is found that the emission profile in Fig. 5(a) is symmetrical with respect to both Z axis and Y axis. But the FWHMs of emission profile in Z axis and Y axis are slightly larger than those of the experimental images. The reason should be the difference in observation angle, which is 60° in the experiment (as shown in Fig. 1) while 90° in the simulation. This difference makes the FWHM in the simulation larger than the experimental result.

The simulated electron density and ion density at 2.2 ms after T_0 are shown in Fig. 6. It is obvious that the distribution of electron density and ion density have a large difference between them. In Fig. 6(a), the distribution of electron density has a similar structure to the distribution of emission as shown in Fig. 5(c). This similarity confirms that the emission is mainly determined by the electrons and distribution of emission can be used to represent the distribution of electron density in the plasma. In Fig. 6(a), the maximum electron density is on the left side and electron density decreases in the Z-axis direction gradually. The maximum electron density on the right side is about 2×10^{11} cm^{-3}, which is only about 1/5 of the initial maximum electron density.

In Fig. 6(b), it is found that the distribution of ion density is symmetrical with respect to the Y axis and the ion density is much lower in the middle for each given Y value. Because the SMB density is much higher in the center and much more ions are knocked down there. The maximum ion density is about 1×10^{12} cm^{-3}, which is almost equal to the initial maximum ion density. But the area where the ion density reaches a maximum value, is in a range of 70 mm–80 mm (Y axis) rather than the radial center ($Y = 50$ mm), indicating that the ions are knocked down about 20 mm–30 mm along the Y axis. There exists an area on the top side where only few ions are left, indicating that the ions there are knocked down completely. To conclude, it is found by simulation that the ions are knocked down about 20 mm–30 mm along the Y axis by the high-density SMB, and the interaction area is filled with lots of atoms and fewer electrons, indicating that the plasma are extinct in the interaction.

3.3. Plasma influenced by medium-density SMB

In the skimmer setup of 10 mm, the SMB density decreases to the order of 10^{13} cm^{-3}, which is about 30% of the SMB density in the skimmer setup of 5 mm in Subsection 3.2. Consequently, the SMB can only affect the plasma column but cannot make it extinct. A complete process of interaction is shown in Fig. 7. Figure 7(a) shows the SMB influenced plasma column at 0.3125 ms after T_0, and figure 7(b) shows the image when the emission reaches a maximum intensity at 1.25 ms after T_0. The structure found in Fig. 7 is similar to that shown in Fig. 4, except the fact that the time needed to reach the maximum emission intensity is longer, and the FWHM in the Z-axis direction is obviously larger. Because the SMB density is smaller while the FWHM of the profile distribution is much larger for the skimmer setup of 10 mm, and much longer time is needed to inject the same quantity of SMB atoms and to have the same emission intensity.

Figures 7(a)–7(c) show that the SMB affects the plasma column continually and the distribution of plasma density is changed accordingly. The emission center shifted to the left side in Figs. 7(b) and 7(c). And the emission intensity increases with the time increasing from 0.3125 ms to 1.2500 ms while decrease from 1.2500 ms to 3.1250 ms. In Fig. 7(d), the emission is much lower at the end of the gas jet, but the plasma is not extinct for the medium-density SMB, indicating that there are still some electrons left in the interaction area.

The simulated electron density and ion density at 3 ms after T_0 are shown in Fig. 8. In Fig. 8(a), the electron density decreases along the Z axis because of the supplement from plasma source and the loss from emission. And the maximum electron density is on the left side and it is about 1×10^{12} cm^{-3}, which is almost equal to the initial maximum electron density. Moreover, the maximum electron density in

the right edge is about 4×10^{11} cm^{-3}, which is still about 1/3 initial maximum electron density. This result indicates that in the whole interaction process, the medium-density SMB can change the distribution of electron density by emission but cannot make the plasma extinct completely.

In Fig. 8(b), the distribution of ion density is symmetrical with respect to the Y direction because there is no supplement from plasma source. The ions on the top side are knocked down about 20 mm along the Y axis by the SMB and the shifted distance of ion is shorter than the result of Fig. 6(b). And the maximum ion density is about 1×10^{12} cm^{-3}, which is almost equal to the initial maximum ion density. These results indicate that the variation of ion density is smaller in the interaction with medium-density SMB than with the high-density SMB.

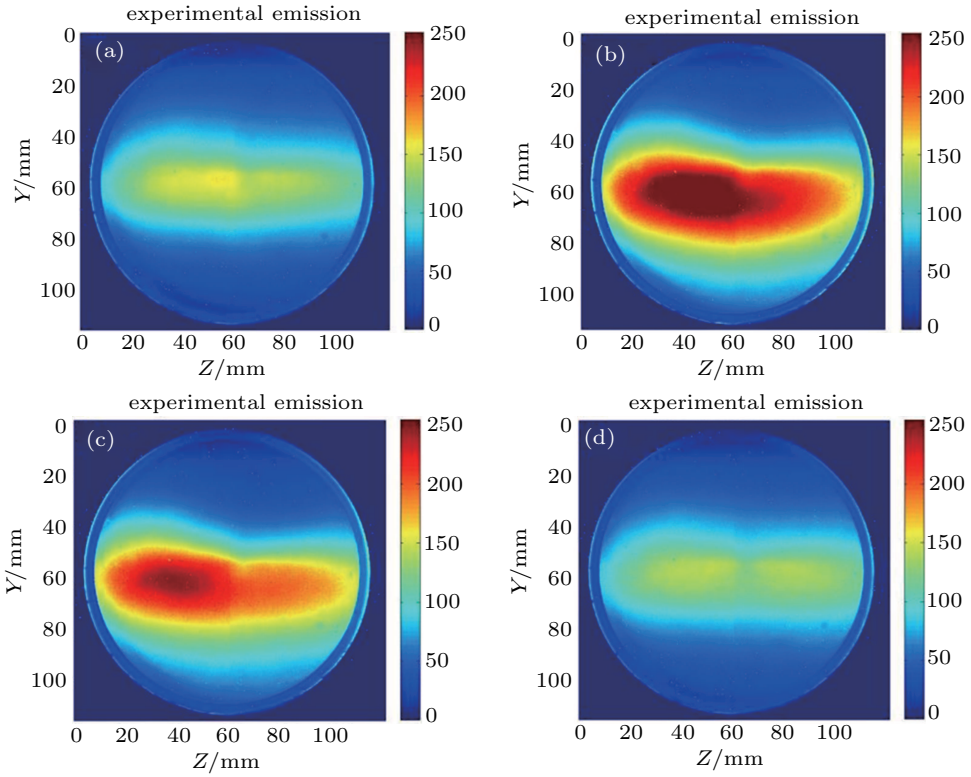


Fig. 7. A series of experimental emission images for medium-density SMB. Distance between nozzle and skimmer is 10 mm, stagnation pressure 50 bar, and central density of SMB about 8.48×10^{13} cm^{-3}, RF power 1000 W, initial central plasma density about 1.97×10^{12} cm^{-3}, at time (a) 0.3125 ms, (b) 1.2500 ms, (c) 2.1875 ms, and (d) 3.1250 ms after SMB has hit plasma column and exposure time of each image is 0.3125 ms.

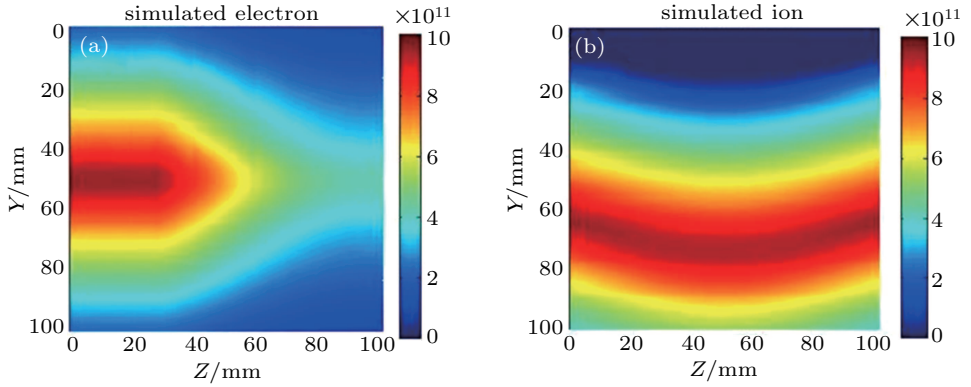


Fig. 8. Simulated distribution of (a) electron density and (b) ion density at 3 ms for medium-density SMB. Distance between nozzle and skimmer is 10 mm, stagnation pressure 50 bar, and RF power 1000 W.

3.4. Plasma slightly influenced by low-density SMB

When the distance between the nozzle and skimmer is fixed at 15 mm, the SMB density decreases to 10^{12} cm^{-3}, which is smaller than or equal to the electron density in plasma. In this case, the electron distribution is hardly influenced by the SMB. A series of experimental emission images is shown in Fig. 9. It is found that the structure is similar to that shown in Fig. 3(a) when there is no gas jet, indicating that the low-density SMB can hardly change the distribution of electron density. The emission intensity almost keeps con-

stant in the four images from 0.3125 ms to 3.125 ms, but it is still much stronger than the emission intensity in Fig. 3(a) obviously. In addition, the emission intensity on the left side is slightly higher than on the right side. This result indicates that on the left side more electrons are supplemented than on the right side in the interaction.

The simulated distribution of electron density and ion density at 1.2 ms after T_0 are shown in Fig. 10. It is found in Fig. 10(a) that the electron density is almost uniform in the Z-axis direction. but it decreases only slightly in the right edge. It is the reason why the emission intensity on the right side is weaker than on the left side as shown in Fig. 9. The maximum electron density is about 2.6×10^{12} cm^{-3} in Fig. 10(a), which is almost equal to the initial electron density. Moreover, this result indicates that the distribution of electron density keeps almost constant during the whole interaction with the low-density SMB.

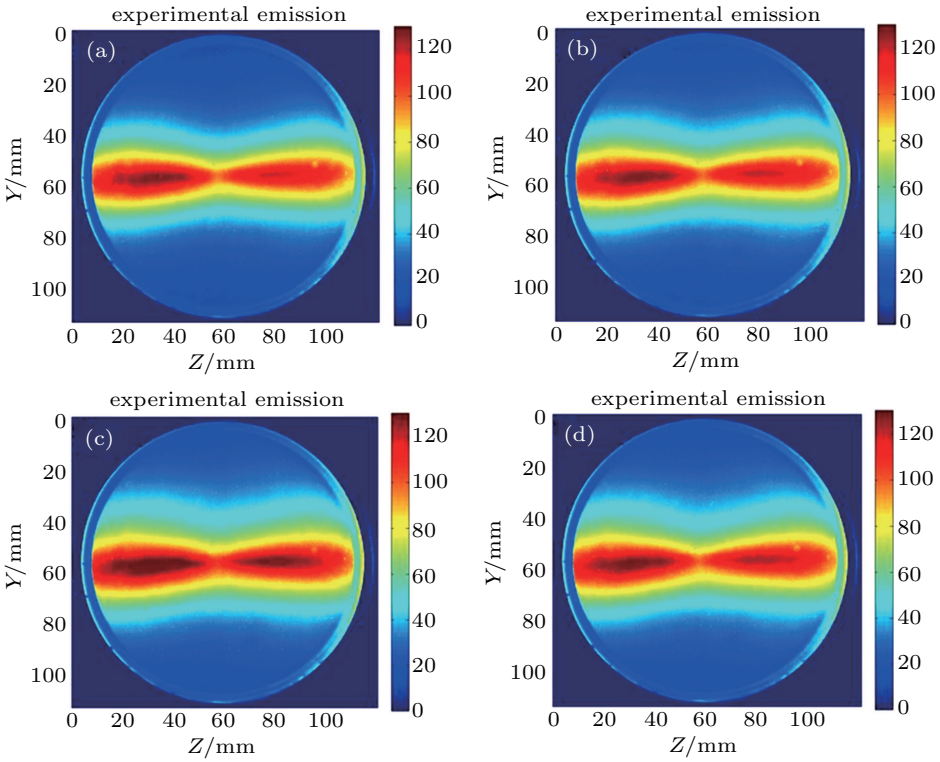


Fig. 9. A series of experimental emission images for low-density SMB. Ddistance between nozzle and skimmer is 15 mm, stagnation pressure 50 bar, central density of SMB about 2.73×10^{13} cm^{-3}, RF power 2500 W, initial central plasma density about 7×10^{12} cm^{-3}, at time (a) 0.3125 ms, (b) 1.2500 ms, (c) 2.1875 ms, and (d) 3.1250 ms after SMB has hit plasma column, and exposure time for each image is 0.3125 ms.

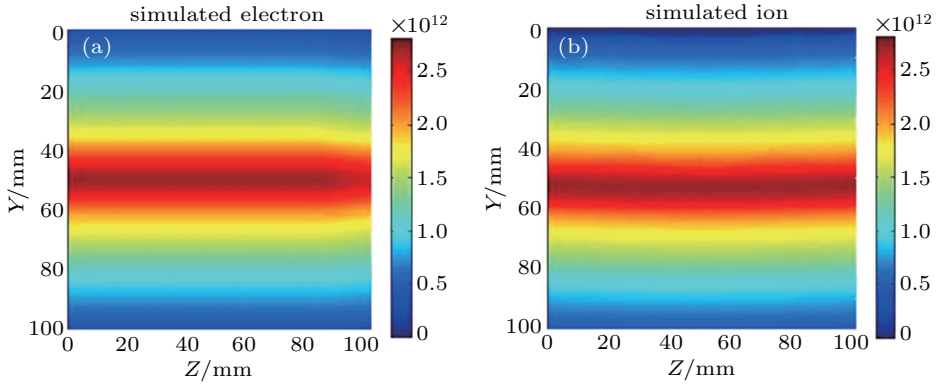


Fig. 10. Simulated (a) electron density and (b) ion density at 1.2 ms for low-density SMB. Distance between nozzle and skimmer is 15 mm, stagnation pressure 50 bar, RF power 2500 W, and central density of SMB about 2.73×10^{13} cm^{-3}.

Furthermore, in Fig. 10(b) the ion density distribution is slightly different from the distribution of electron density. The distribution of ion density is symmetrical with respect to the Y-axis direction. And the ions on the top side are knocked down about 5 mm along the Y axis by the low-density SMB. This distance is much shorter than the result obtained by high-density SMB in Fig. 6(b) and medium-density SMB in Fig. 8(b). The maximum ion density is about 2.6×10^{11} cm^{-3} at the center position ($Y = 50$ mm), indicating that the distribution of ion density keeps almost constant in the process of

interaction. This should be one effective method to diagnose the distribution of electron density in the plasma, where the electron density in the SMB range can be effectively acquired based on the emission intensity image. To make this diagnostic technique more adequate, the atom density of SMB should be smaller than or equal to that of electron density in the plasma.

4. Summary

The interaction between the argon SMB and the argon low-temperature plasma column is studied in this experiment by a high-speed camera. The whole process of the interaction including the influence and extinction caused by the SMB is recorded by a series of emission images. Furthermore, a simple simulation is conducted and the obtained results explain the distribution of plasma density and its variation in the interaction well. It is found that this interaction can lead both plasma and SMB to change. For the injection of high-density SMB, the distribution of plasma density is strongly changed and the plasma can be extinct temporally, while the SMB flux decreases only slightly in the whole interaction process. For the injection of low-density SMB, the distribution of plasma density is hardly influenced, and the emission intensity is proportional to the electron density. Thus, it can become an effective method to diagnose the distribution of electron density in the plasma. These conclusions could help understand in depth the relationship between the SMB density and injection depth of SMBI in the Tokamak. Moreover, these results are valuable for studying in depth the interaction between SMB and plasma, and the physics of atom and plasma.

References

[1] Xiao J S, Yang Z J, Liu M H, Zhuang G, Pan X M, Zhang C and Wang Z J 2015 *J. Fusion Energy* **34** 1020

[2] Sajjad S, Gao X, Ling B, Bhatti S H and Ang T 2009 *Phys. Lett. A* **373** 1133

[3] Yuan J B, Yuan B D, Xu M, Yu Y, Nie L, Ke R, Wang Z H, Gong S B, Wu T, Wu Y F, Long T, Wang H J, Liu H and Yue W 2019 *Plasma Sci. Technol.* **21** 084002

[4] Baylor L R, Jernigan T C, Combs S K, Houlberg W A, Murakami M, Gohil P, Burrell K H, Greenfield C M, Groebner R J, Hsieh C L, La Haye R J, Parks P B, Staebler G M, Team D I I I D, Schmidt G L, Ernst D R, Synakowski E J and Porkolab M 2000 *Phys. Plasmas* **7** 1878

[5] Yao L H, Feng B B, Feng Z, Luo J L, Dong J F, Yan L W and Hong W Y 2001 *Plasma Sci. Technol.* **3** 589

[6] Zhou Y L, Wang Z H, Xu M, Wang Q, Nie L, Feng H and Sun W G 2016 *Chin. Phys. B* **25** 095201

[7] Rajeev R, Raja S V, Trivikram T M, Rishad K P M and Krishnamurthy M 2013 *J. Appl. Phys.* **114** 083112

[8] Liu D, Han J F, Chen Z Y, Bai L X and Zhou J X 2016 *Rev. Sci. Instrum.* **87** 123504

[9] Chen Z Y, Li M, Zhou M L, Liu D, Qu G F, Wang Y Z and Han J F 2019 *J. Fusion Energy* **38** 228

[10] Yao L H, Zhou Y, Cao J Y, Feng B B, Feng Z, Luo J L, Dong J F, Yan L W, Hong W Y, Li K H, Cui Z Y, Liu Y, Wang E Y, Yan J C and HL-1M Team 2001 *Nucl. Fusion* **41** 817

[11] Yao L H, Feng B B, Chen C Y, Shi Z B, Yuan B S, Zhou Y, Duan X R, Sun H J, Lu J, Jiao Y M, Ni G Q, Lu H Y, Xiao W W, Li W, Pan Y D, Hong W Y, Ran H, Ding X T and Liu Y 2007 *Nucl. Fusion* **47** 1399

[12] Yu D Y, Chen C Y, Yao L H, Feng B B, Han X Y, Yang L M, Zhong W L, Zhou Y, Zhao K J, Huang Y, Liu Y, Yan L W, Yang Q W, Dong J Q and Duan X R 2010 *Nucl. Fusion* **50** 035009

[13] Yao L H, Zhao D W, Feng B B, Chen C Y, Zhou Y, Han X Y, Li Y G, Jerome B and Duan X R 2010 *Plasma Sci. Technol.* **12** 529

[14] Yuan X L, Li J G, Wu J H, Li J H, Chen Y, Zhuang H D, Zhou Y, Zheng X W and Hu J S 2018 *Fusion Eng. Des.* **134** 62

[15] Takenaga H, Miyo Y, Bucalossi J, Marty V, Urano H, Asakura N, Nishiyama T, Sasajima T, Masaki K and Kaminaga A 2010 *Nucl. Fusion* **50** 115003

[16] Shi Z B, Yao L H, Ding X T, Duan X R, Feng B B, Liu Z T, Xiao W W, Sun H J, Li X, Li W, Chen C Y and Jiao Y M 2007 *Acta Phys. Sin.* **56** 4771 (in Chinese)

[17] Wu X K, Li H D, Wang Z H, Feng H and Zhou Y L 2017 *Chin. Phys. B* **26** 065201

[18] Wang Z H, Xu X Q, Xia T Y and Rognlien T D 2014 *Nucl. Fusion* **54** 043019

[19] Zhou Y L, Wang Z H, Xu X Q, Li H D, Feng H and Sun W G 2015 *Phys. Plasmas* **22** 012503

[20] Wang Y H, Guo W F, Wang Z H, Ren Q L, Sun A P, Xu M, Wang A K and Xiang N 2016 *Chin. Phys. B* **25** 106601

[21] Liu H 2018 *Design and Construction of Linear Experimental Advanced Device*, MS dissertation (Hefei: University of Science and Technology of China) (in Chinese)

[22] Anderson C A, Hopkins M B and Graham W G 1990 *Rev. Sci. Instrum.* **61** 448

[23] Tachibana K, Nishida M, Harima H and Urano Y 1984 *J. Phys. D: Appl. Phys.* **17** 1727

[24] Shinohara S, Hada T, Motomura T, Tanaka K, Tanikawa T, Toki K, Tanaka Y and Shamrai K P 2009 *Phys. Plasmas* **16** 057104

[25] Shinohara S, Nishida H, Tanikawa T, Hada T, Funaki I and Shamrai K P 2014 *IEEE T. Plasma Sci.* **42** 1245

[26] Katsonwas K, Berenguer Ch, Kaminska A and Dudeck M 2011 *Int. J. Aerosp. Eng.* **2011** 896836

[27] Boffard J B, Chiaro B, Weber T and Lin C C 2007 *Atom. Data Nucl. Data* **93** 831

[28] Barata J A S 2007 *Nucl. Instrum. Method B* **580** 14